Direct Acceleration of an Annular Attosecond Electron Slice Driven by Near-Infrared Laguerre–Gaussian Laser

C. Jiang[1, 2, 3], W. P. Wang[1, *], S. Weber[4,5], H. Dong[1, 3], Y. X. Leng[1,2], R. X. Li[1, 2] and Z. Z. Xu[1, 2]

[1]State Key Laboratory of High Field Laser Physics and CAS Center for Excellence in Ultra-intense Laser Science, Shanghai Institute of Optics and Fine Mechanics, Chinese Academy of Sciences, Shanghai 201800, China.

[2]School of Physical Science and Technology, ShanghaiTech University, Shanghai 201210, China.

[3]University of Chinese Academy of Sciences, Beijing 100049, China.

[4]Institute of Physics of the ASCR, ELI-Beamlines Project, 18221 Prague, Czech Republic.

[5]School of Science, Xi'an Jiaotong University, Xi'an 710049, China.

Abstract A new near-infrared direct acceleration mechanism driven by Laguerre–Gaussian laser is proposed to stably accelerate and concentrate electron slice both in longitudinal and transversal directions in vacuum. Three-dimensional simulations show that a 2-μm circularly polarized LG_p^l($p = 0$, $l = 1$, $\sigma_z = -1$) laser can directly manipulate attosecond electron slices in additional dimensions (angular directions) and give them annular structures and angular momentums. These annular vortex attosecond electron slice is expected to have some novel applications such as in the collimation of antiprotons in conventional linear accelerators, edge-enhancement electron imaging, structured *x*-ray generation, and analysis and manipulation of nanomaterials.

Key words: Annular electron slice , Laguerre–Gaussian lasers , Direct laser acceleration , Near-infrared laser

*wangwenpeng@siom.ac.cn;

1. Introduction

With the rapid development of ultra-short ultra-intense laser technology, the laser intensity can be increased up to 10^{22} W/cm^2 in petawatt laser facilities [1-4]. Such laser pulses can be used to apply extremely high electromagnetic fields to accelerate electron beams to GeV levels [5, 6]. Thus far, two main accelerating mechanisms have been proposed: direct laser acceleration (DLA) [7] and indirect laser acceleration (ILA) [8-11]. In the ILA mechanism, electron accelerations are typically driven in a plasma environment, such as in the laser wakefield acceleration (LWFA) regime, where the accelerating gradients are larger than 100 GV/m [12]. Electrons can be captured and accelerated to several GeVs with less energy spread and a charge of ~0.1 nC in the LWFA regime [13-15]. In the DLA mechanism, electrons are directly accelerated by the laser field itself, with the accelerating gradients reaching an order of 10 TV/m. Compared with the ILA mechanism (such as LWFA), the DLA mechanism yields a more compact gradient because it has a limited dependence on the plasma environment. As such, this method has attracted considerable attention [16-21].

However, the DLA mechanism has a limitation in that it cannot stably accelerate a large number of electrons for a long time. This is because the electrons are typically accelerated by the ponderomotive force $F_p = -e^2\nabla E^2/4m_e\omega_L^2$ in the linear limit ($E \ll m_e c^2/e$) and by $F_{pN} = -m_e c^2\nabla\gamma$ in the nonlinear regime[22], where e is the charge of the electron, E is the electric field amplitude, m_e is the mass of the electron, ω_L is the laser frequency, c is the speed of light in vacuum, and $\gamma \approx [1 + (eE/m_e\omega_L c)^2]^{1/2}$ is the relativistic factor associated with the quiver motion of electrons. An approximate Gaussian distribution of F_p or F_{pN} driven by a conventional Gaussian laser pulse will push the electrons to both sides of the laser beam axis, resulting in a scenario where fewer electrons are locked in the accelerating phase until they finally disappear. This is much different from that observed in the LWFA mechanism, where electrons are accelerated in ionized "bubble-like" plasma channels driven by an ultra-intense Gaussian laser pulse. GeV-level electron beams can be realized by accelerating the electrons in the longitudinal charge-separation field and constraining them via the transverse electric field in the bubble. For a more efficient electron acceleration in the DLA regime, the transverse confining effects should also be considered.

Fortunately, Laguerre–Gaussian (LG) lasers can provide a confining force to manipulate matters, such as proton [23-26], electron [27-32] and positron [33], in the transverse direction. Previously, optical tweezers or optical wrenches driven by LG lasers have been applied to concentrate and rotate micrometer matter in the nonrelativistic regime [34, 35]. With the development of advanced laser facilities [2, 36], an LG laser has the potential to be extended to the relativistic regime [37-41]. Now the highest intensity of the LG laser can reach up to 6.3×10^{19}W/cm^2 by using the reflected phase plate on the petawatt laser facility in experiments [26]. The relativistic LG laser is expected to open new doors for particle manipulation in the DLA regime, because the hollow intensity distribution of the LG laser may result in the formation of a transverse potential well about the beam axis, similar to the charge-separated field structure in the bubble regime of LWFA [42-45]. It is believed that electrons can be accelerated in a concentrated manner in a new type of "bubble" regime, to overcome some of the drawbacks of Gaussian-laser driven DLA to a certain extent [46-50].

In this letter, we report an annular electron slice obtained for the first time using a near-infrared circularly polarized (CP) LG_p^l ($p = 0$, $l = 1$, $\sigma_z = -1$) laser in 3D particle-in-cell (PIC) simulations.

We found that a 2-μm infrared LG laser can provide a stable accelerating phase in the longitudinal direction and a concentrating force in the transverse direction, forming a "bubble", similar to the case observed in the LWFA mechanism. Finally, a single attosecond electron slice was successfully accelerated up to hundreds of megaelectron volts in the DLA regime, which is explained using a single-particle theoretical model. More importantly, the electron slice structure can be changed from a disk to an annular shape by accurately tuning the carrier-envelope phases (CEPs) of the LG laser. The novel annular attosecond electron slice captured in a "bubble" is compact and is expected to have potential applications such as in the collimation of energetic particles such as antiprotons in conventional linear accelerators [51], edge-enhancement electron imaging [52], structured x-ray generation [53], and analysis and manipulation of nanomaterials [54].

2. Simulation results

Three-dimensional PIC simulations were carried out to investigate the formation and evolution of an annular electron slice driven by an intense near-infrared LG laser pulse. The 3D PIC simulations in this work were actualized with the code EPOCH[55]. Each simulation used about 6.5 $\times$ 10^3 core hours on a parallel machine based on CentOS7 system. We employed the CP LG_p^l (p = 0, l = 1, σ_z = −1) laser mode, which can be expressed as follows:

$$\boldsymbol{E}_{\perp} = E_0 \sqrt{\frac{2p!}{\pi(p+l)!w(x)}} \left[\frac{r\sqrt{2}}{w(x)}\right]^l exp\left[\frac{-r^2}{w^2(x)}\right] L_p^l\left[\frac{2r^2}{w^2(x)}\right] \exp(il\phi)$$

$$\exp\left[\frac{ik_0 r^2 x}{2(x^2+x_R^2)}\right] exp\left[-i(2p+l+1)tan^{-1}\left(\frac{x}{x_R}\right)+\psi\right][\boldsymbol{e_y} + exp\left(\frac{i\pi\sigma_z}{2}\right)\boldsymbol{e_z}], \qquad (1)$$

where $E_0 = a_0 m_e \omega_L c/e$ is the peak amplitude of the electric field, a_0 = 25 is the normalization amplitude of the laser pulse (corresponding to a laser intensity $I \sim 2\times10^{20}$ W/cm^2), m_e is the mass of the electron, ω_L is the laser frequency, c is the speed of light in vacuum, and e is the charge of the electron; l is the number of azimuthal phase cycles, and p + 1 denotes the number of radial nodes; $w(x) = w_0(1 + x^2/x_R^2)^{1/2}$ is the beam waist with w_0~ 20 μm (full-width at half-maximum, FWHM) being the diameter of the focus spot, $x_R = \pi w_0^2/\lambda$ is the Rayleigh length, L_p^l is the generalized Laguerre polynomial, ϕ is the azimuthal angle, and $(l + 2p + 1)\tan^{-1}(x/x_R)$ is the Gouy phase of the mode. The laser wavelength is λ = 2 μm, and the laser duration is 10 femtoseconds (fs) (FWHM). The foil thickness is 100 nm, corresponding to regions of 20 μm < x < 20.1 μm, −27 μm < y < 27 μm, and −27 μm < z < 27 μm. The foil density is n_e = 0.5n_c, where $n_c = \varepsilon_0 \omega_L^2 m_e/e^2$ (where ε_0 is the dielectric constant). Such ultrathin target foil may be available by using the few-nanometre carbon foil[56, 57]. The foil is assumed to be ionized to protons and electrons before the laser reaches the target. The size of the simulation box is 30 μm (x) × 60 μm (y) × 60 μm (z) with 1200×1000×1000 cells, and total 1.2 × 10^9 electrons and 1.2 × 10^9 protons are uniformly distributed in foil in the initial time. The initial temperature of plasma was zero for cold target in our case. The simulation uses a moving window which starts at t = 8T with light speed, where $T = \lambda/c$ is laser cycle.

In the simulation, the near-infrared CP LG laser pulse is incident on the target from the left [see Fig. 1(a)]. The laser beam arrives at the front surface of the target at t = 11T. The electrons are quickly pushed away from the target area because the ponderomotive force is much greater than the

charge-separated field force between the electrons and protons in this case [58-61]. The electrons are then continuously accelerated through the DLA mechanism, as shown in Fig. 1(b). On the one hand, the electrons are completely locked and accelerated up to 210 MeV at $t = 88T$ in the accelerating phase of the longitudinal electric field [see Fig. 1(c)]. On the other hand, an electron slice can be concentrated within ~2° [see Fig. 1(d)] in the transverse direction because of the formation of a transverse potential well about the beam axis (x axis), thus concentrating the electron toward the center to a certain extent [see Figs. 1(e)]. The field structure formed in the transverse and longitudinal directions in our case is similar to the formation of plasma bubbles in LWFA [42, 62]. The only difference is that the accelerating phase is ahead of the decelerating phase in the "bubble," and the size is determined by the wavelength of the LG laser in our case.

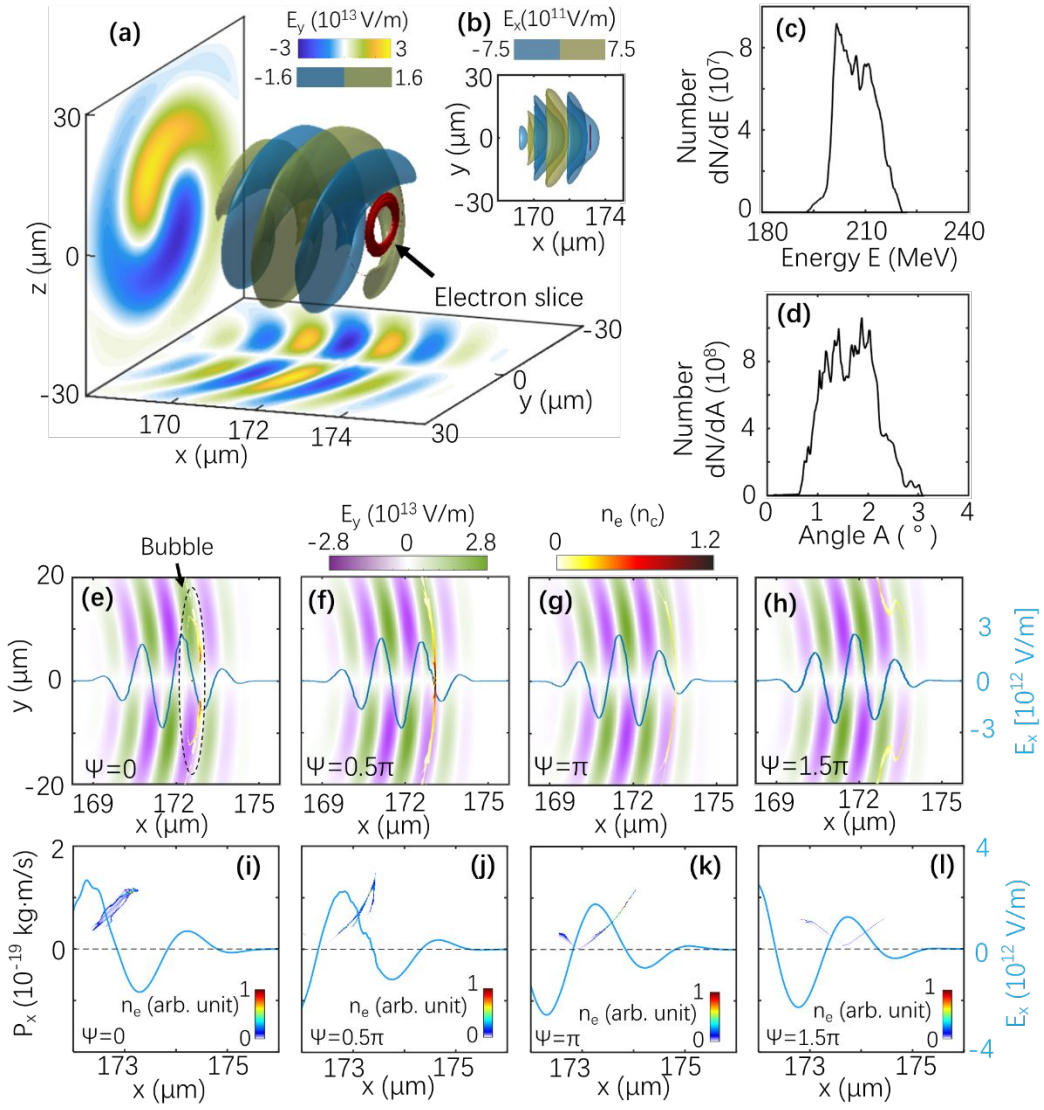

FIG. 1 Electron slice and LG laser field in PIC simulation. (a) Sketch of an electron slice driven by an LG laser. The red donut indicates the isosurface of the electron slice with $n_e = 0.3n_c$ for the carrier-envelope $\Psi = 0$. The blue and yellow translucence isosurfaces indicate the distributions of the LG laser field E_y. (b) Distributions of the laser electric field E_x and electron slice in the x-y plane. (c), (d) Energetic spectra and angular distribution for the electrons in the regions of 173 μm < x < 183

μm, $0 < r < 8$ μm at $t = 88T$. Density distributions of the electron slice for different carrier-envelope phases (e) $\Psi = 0$, (f) 0.5 π, (g) π and (h) 1.5 π at $88T$. Corresponding phase-space distributions of the electrons and amplitude of E_x (blue line) on the x-axis at $t = 88T$ are plotted for (i) $\Psi = 0$, (j) 0.5 π, (k) π and (l) 1.5 π.

Figs. 1(e)-1(h) show that the density distribution shapes of the electron slices at $t = 88T$ can be changed from disk to annular by varying the CEP of the LG laser. For $\Psi = 0$, the density distribution of the electrons is modulated to an annular shape with an inner diameter of ~10 μm, as shown in Figs. 1(a), 1(b), and 1(e). This annular electron slice can be accelerated up to 220 MeV with a slice thickness of 0.2 μm (corresponding to ~670 attoseconds) at $t = 88T$, as shown in Fig. 1(e). The total charge of such an annular electron slice can reach up to ~0.19 nC. By contrast, an electron disk is generated at the beam center when $\Psi = 0.5\pi$, as shown in Fig. 1(f). In the other two cases shown in Figs. 1(g) and 1(h), the electron slice is dispersed. The electron motion seems to have a close relationship with the phase structure in the laser field.

To explain the effects of CEP on the formation of the annular electron slice [see Fig. 1(a) and 1(e)], both the transverse [Fig. 2(a)–2(d)] and longitudinal electric fields [Fig. 2(e)] in one laser cycle are discussed. It should be noted that most electrons travel along the direction of the laser and the transverse electron field $|E_\perp|$ is larger than $|v_x \times B_\perp|$ in simulations for our cases. So, we approximately consider that the electric field plays the main roles for the formation of electron bunch. The decelerating phase and accelerating phase for longitudinal electric field E_x are marked in Fig. 2(e). When the LG laser pulse incidents on the target, the electrons are first concentrated by the dispersing electric field similar to point i [see Fig. 2(a)] and subsequently rotated by the clockwise field similar to point ii [see Fig. 2(b)], indicating that the electrons can be continuously concentrated in the transverse direction at the beginning of the interaction (from i to ii). Such process can be clearly shown in the evolution of electron slice from $t = 11T$ to $t = 25T$ [see Fig. 2(f) and 2(g)]. The electrons are then dispersed by the concentrating electric field similar to point iii [see Fig. 2(c)] corresponding to $t \sim 35T$ [see Fig. 2(h)]. It can be found that the electron slice is shortly manipulated by a dispersing force (around t ~ 5T), forming an annular structured slice. The longitudinal field increases up to $E_x \sim 1.67\times10^{12}$ V/m at point iv, where most of the electrons can be locked in such a wide accelerating phase. The electron slice is further manipulated by the rotated electric field force and the weak inward electric field force in the accelerating region for a longer time [see Fig. 1(e)(i)], resulting in a stable annular slice, as shown in Fig. 1a. Compared with the case $\Psi = 0$ in Fig. 2(e), the laser field E_x is much lower in the decelerating region (from i to iii) in the case of $\Psi = 0.5\,\pi$ [see Fig. 1(j)]. Thus, the process of dispersing by the concentrating electric field [see Fig. 2(c)] and decelerating by E_x is shorter than case of $\Psi = 0$, resulting in a higher density distribution in the case of the disk structure on the beam axis (x axis).

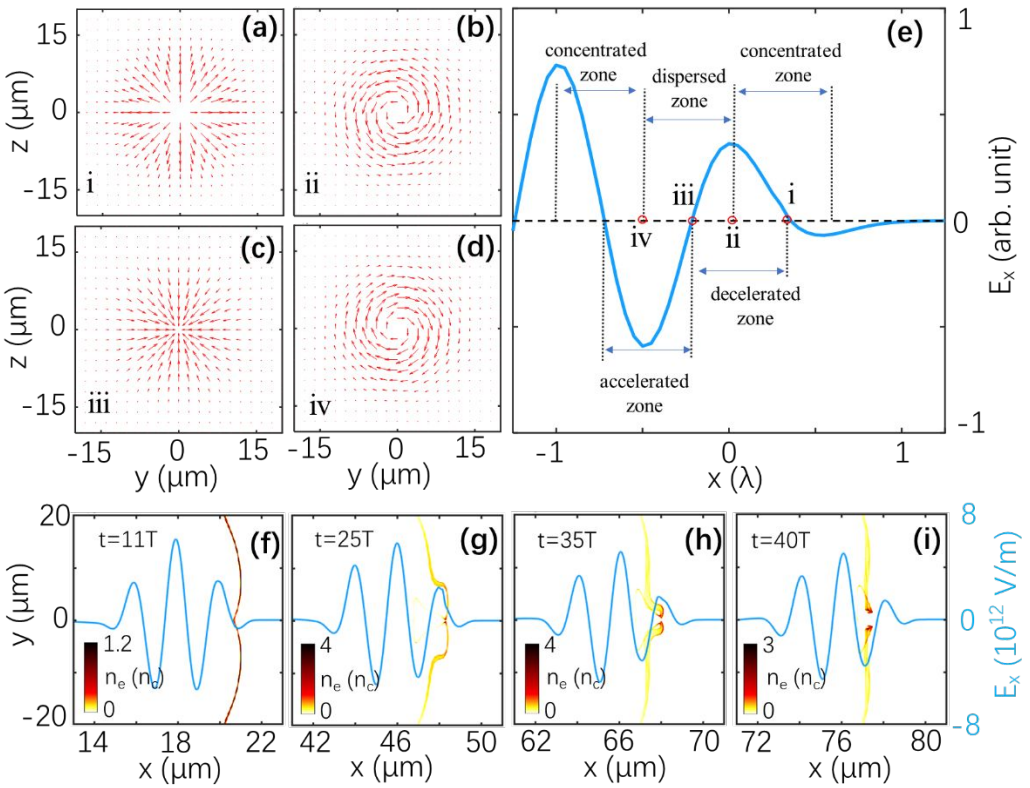

FIG. 2 Structure of electric fields of CP LG laser and phase-space distribution of electrons. Normalized vector plots of the transverse electric fields in one laser cycle for (a) i, (b) ii, (c) iii, and (d) iv marked in (e). (e) Normalized amplitude of E_x (blue line) on the x-axis for $\Psi = 0$. Density distributions of electron slice and amplitude of E_x (blue solid) for $\Psi = 0$ at (f) $t = 11T$, (g) $t = 25T$, (h) $t = 35T$ and (i) $t = 40T$ are plotted.

In the other two cases shown in Figs. 1(k) and 1(l), the electrons are first dispersed by the transverse fields. Although they lie in the accelerating phase at the beginning of the interaction, the amplitude of E_x is much lower than in the cases shown in Figs. 1(i) and 1(j). Therefore, these electrons will easily slide into the decelerating phase and undergo considerable dispersion in the longitudinal direction. Finally, fewer electrons are formed about the beam axis, much different from the cases shown in Figs. 1(i) and 1(j). This indicates that the formation of a concentrated electron slice with high energy requires two conditions in our case. One the one hand, the transverse electric fields should be concentrated on the electrons at the beginning of the interaction. One the other hand, the electrons should move into the large and stable accelerating phase as soon as possible, so that they can remain in a concentrated state in the ensuing acceleration process. If the transverse rotating fields just lie in the accelerating phase, the annular electron slice can be successfully maintained, as shown in Figs. 1(a) and 1(i).

3. Theoretical analysis

To explain the simulation results, a single-particle model is employed to show the dynamic motion of a single electron in the LG laser field. The fundamental motion of the electrons can be described by the equation $d\boldsymbol{p}/dt = e(\boldsymbol{E} + \boldsymbol{v} \times \boldsymbol{B})$, where $\boldsymbol{p} = m_e \gamma \boldsymbol{v}$ is the particle momentum, $\boldsymbol{E}$ is the electric field intensity, and $\boldsymbol{B}$ is the magnetic intensity. Since the azimuthal electromagnetic

fields exist for a CP LG laser pulse, it becomes challenging to find an analytical solution for the single-particle motion. A feasible method is solving the equations numerically. $\boldsymbol{E}_\perp = E_y\boldsymbol{e_y} + E_z\boldsymbol{e_z}$ is described in Eq. 1, where E_y and E_z displace with $\pi/2$ at the propagation phase. Here, the longitudinal electric field is obtained from the Poisson's equation, $E_x = -(i/k)\nabla \boldsymbol{E}_\perp$:

$$E_x = \frac{i}{k}\left[\left(\frac{z}{r^2} - \frac{2z}{w(x)} + il\frac{y}{r^2} + \frac{ikx}{x^2 + x_R^2}\right)E_z + \left(\frac{y}{r^2} - \frac{2y}{w(x)} - il\frac{z}{r^2} + \frac{ikx}{x^2 + x_R^2}\right)E_y\right]. \quad (2)$$

For the mode of CP LG_p^l ($p = 0$, $l = 1$, $\sigma_z = -1$), there is a longitudinal electric field E_x at the beam center. The maximum value of E_x is ~6 TV for $a_0 = 25$ in our case. The magnetic fields derive from the electric fields based on Maxwell's equation $\boldsymbol{B} = (i/ck)\nabla \times \boldsymbol{E}$.

To understand the phase-locked movement of the electron slice in the PIC simulations, the single-particle model was applied for four typical electrons at $x = 3.8$ μm, $y = \pm 1$ μm, and $z = \pm 1$ μm, where the location of the simulation phase-locked region, shown in Fig. 1(a), is considered. According to the angular distribution of electrons, the transverse velocity v_r is much lower than v_x ($v_r/v_x < 3\%$ for most electrons). The $v_r = 0$ is used for simplicity. And the initial longitudinal velocity of the electrons is set to 0.999c, because the energy of most of the electrons that just enter the accelerating phase is approximately 11 MeV when $v_x = 0.999c$ at $t = 42T$ in the simulations. The parameters of the electromagnetic field are the same as when $\Psi = 0$, as shown in Fig. 1(e), in the PIC simulation. The 3D trajectories of the electrons show that they could remain in the acceleration phase of the CP LG laser for a distance more than 60 μm, as shown in Fig. 3(a). It should be noted that the electron slice gains hundreds of megaelectron volts of energy from such a phase-locked acceleration in the PIC simulation. In addition, the electrons undergo a right-handed rotation about the x-axis [see Fig. 3(c)], consistent with the vector distributions of the transverse electric fields in the accelerating phase [see Figs. 2(d)]. In PIC simulation, the direction of rotated transverse electric field does not change in the accelerating phase, so that the angular momentum (AM) of electrons can continually increase from negative to positive after $t = 40T$, just as shown in Fig. 3(b). However, the initial AM of the electron is zero in the single-particle model. So, the total AM of the four electrons can only increase from zero to positive in accelerating phase, and the rotation directions of electrons do not change in Fig. 3(c). We assume that the electrons can be rotated by these transverse electric fields [see Fig. 2(b)], as evidenced by the evolution of their AM shown in Fig. 3(b). Therein, the resonance of the AM corresponds to the different rotations (right-handed or left-handed) of the transverse electric fields [see Figs. 2(b), 2(d)].

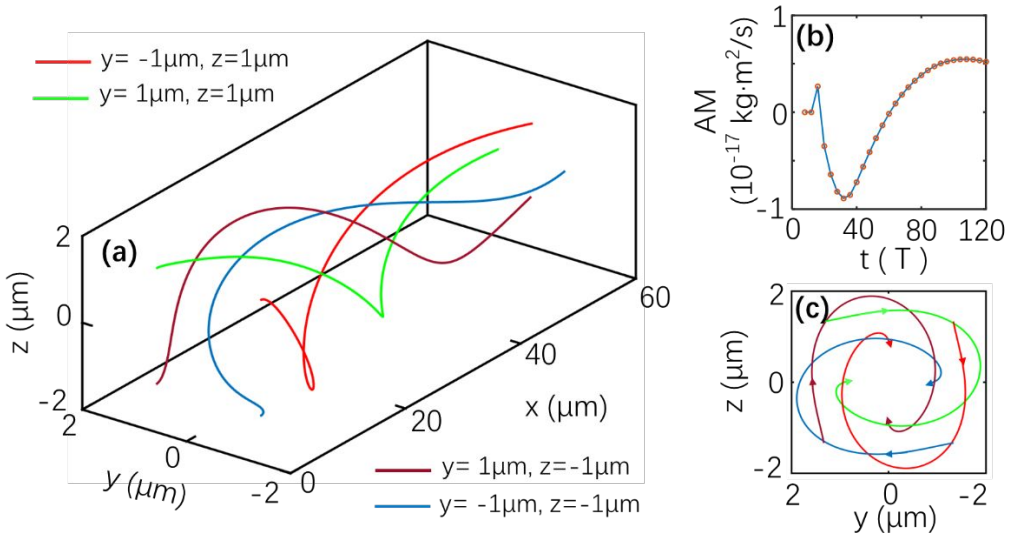

FIG. 3. Trajectories of electrons in single-particle model and AM in PIC simulation. (a) 3D trajectories of electrons at different initial positions of $x = 3.8$ μm [accelerated phase corresponding to point ⅳ in Fig. 2(e)], $y = \pm 1$ μm, and $z = \pm 1$ μm. Here, the electrons have an initial velocity of $v_x = 0.999c$. (b) AM for the electrons in the regions of 0 μm $< x <$ 400 μm, −10 μm $< y <$ 10 μm, and −10 μm $< z <$ 10 μm in PIC simulation with $\Psi = 0$. (c) View of 3D trajectories in the forward direction.

4. Discussion

From the above analyses, we find that a near-infrared LG laser can successfully provide a stable and efficient accelerating phase to generate a single annular attosecond electron slice in the DLA regime. The main reason is that the near-infrared LG laser (λ = 2 μm) can provide a longer accelerating field to stably maintain the annular structure of the electrons up to 853 fs [see Fig. 4(a)]. It should be noted that a small part of the electron beam is dragged into the next accelerating field, where can be concentrated by the transverse electric field, forming a small dot around the beam axis (x axis), just as shown in Fig. 4(a). A clearer annular electron slice may be obtained if we set a solid target to stop the further acceleration of the LG laser in the earlier interacting progress. From Fig. 4(a), the corresponding energy of the electron slice can be further accelerated from ~210 MeV at 88T [see Fig. 1(c)) to ~280 MeV at $t = 128T$ (853 fs) [see Fig. 4(d)]. By contrast, the electron slices are considerably dispersed at 853 fs when the laser wavelength is shorter (λ = 800 nm), as shown in Fig. 4b, and the electrons can only be accelerated up to ~80 MeV due to the easier dephasing effect for the LG laser with a shorter wavelength [see Fig. 4(e)]. More importantly, the angular divergence remains at ~2° [see Fig. 4(g)] over 88T, meaning that an electron slice can be well concentrated in the "bubble," thus overcoming the dispersion problem in the DLA regime when driven by a conventional Gaussian laser pulse [see Figs. 4(c), 4(i)]. Although, the maximum energy can also be accelerated up to ~150 MeV at 853 fs when using a Gaussian laser with λ = 2 μm, the energetic spread is as high as ~30% [see Fig. 4(f)]. In addition, the divergence of the electron slice is 0-7° in the case of the LG laser with λ = 800 nm [see Fig. 4(h)] and 3-6° in the case of the Gaussian laser with λ = 2 μm [see Fig. 4(i)], which is greater than that (~2°) in the case of the near-infrared LG laser with λ = 2 μm [see Fig. 4(g)]. All these comparisons indicate that the near-infrared LG laser

discussed in this letter helps accelerate the electron slice to a higher energy (hundreds of megaelectron volts) with attosecond duration and concentrate it in a smaller divergence angle (~2°). Such high quality of the annular electron slice may have various applications, such as antiprotons in conventional linear accelerators [51], edge-enhancement electron imaging [52], structured x-ray generation [53], and analysis and manipulation of nanomaterials [54], and so on.

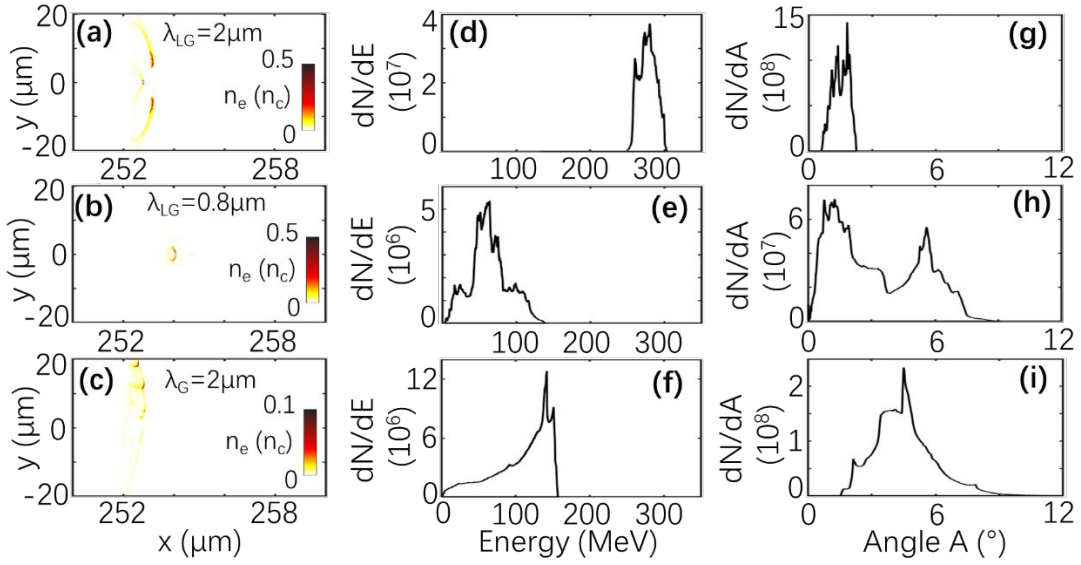

FIG. 4. Comparisons between the cases driven by LG laser and Gaussian laser. Density distributions of electrons at t = 853 fs for LG laser with (a) λ = 2 μm, LG laser with (b) λ = 0.8 μm, and Gaussian laser with (c) λ = 2 μm. (d-f) Energetic spectra and (g-i) angular distribution of the electrons in (a-c), respectively. The electrons in in the regions of 252.8 μm < x < 260 μm, 0 < r < 10 μm are considered for the case in (d) and (g) and the electrons in the regions of 250 μm < x < 260 μm, 0 < r < 20 μm are considered for the cases in (e), (f), (h) and (i).

It should be noted that the longitudinal electric field (E_x) of the LG laser plays an important role to accelerate the electron slice to a high energy in the "bubble" mechanism in this paper, where the charge-separation field between the electron and ion slice is not considered. It is reasonable because the normalized amplitude of the charge-separation field $a_{cs} = \pi n_e l_0$ ~ 0.08 for the initial foil thickness l_0 = 0.05 λ and density n_e = 0.5n_c [60, 61, 63, 64] is much lower the longitudinal amplitude a_x = 1.03 (corresponding to 1.67×10^{12} V/m) for the LG laser used in our case. In this way, the dynamics of the electrons only driven by the LG laser field can be considered in Eq. (2). So, the applicable condition of Eq. (2) is $a_x >> \pi n_e l_0$. Such lower area density of the foil ($n_e l_0$) can be obtained by extending the nano Carbon foil in the realistic experiments. An extending target with initial density distribution of $n_e(x) = n_0(x$ - 20 μm)/L, (20 μm < x < 20.1 μm) and $n_e(x) = n_0$ (20 μm - x)/L, (20.1 μm < x < 20.2 μm) is researched for LG laser with $\Psi = 0$ in the PIC simulations, where n_0 = 0.5 n_c is maximum electron density of target and L = 0.1 μm. The similar annular electron slice can be obtained at t = 88T. We assume that the electron slices can be better formed if the laser ponderomotive force is much larger than charge-separation field $a_{cs} = \pi n_e l_0$, which is determined by the area density of the foil $n_e l_0$. The preplasma may have some effects on the mina structures of the electron slice. But it is not the crucial effects. It is assumed that a thinner foil can work better for the mechanism proposed in this paper, because the smaller charged separation field can be

generated for the thinner foil. However, we should further increase the cell number per laser wavelength to increase the accuracy of the simulation for the thinner foil, which is limited to our present computer source and will be consider in the future. The charge-separation field should be considered in a more complex manner with the increasing of the foil thickness l_0 or density n_e.

5. Summary

In conclusion, a novel annular electron slice driven by a few-cycle near-infrared LG laser is investigated for the first time through 3D PIC simulations. We found that a near-infrared LG laser can provide a "bubble" region, characterized by a longer longitudinal electric field that can stably accelerate the electron slice up to hundreds of megaelectron volts with attosecond duration. The longitudinal field mainly accelerate or decelerate the electrons in the forward direction in our case. And the disk or annular formation of the electron slice can be tuned by the transverse fields in LG laser. A stable formation of the annular election slice needs a proper combination of the longitudinal and transverse fields with different amplitudes, which are just determined by the CEP of LG laser. The annular attosecond electron slice is compact and may have potential applications in the collimation of energetic particles such as antiprotons in conventional linear accelerators, edge-enhancement electron imaging, structured *x*-ray generation, and analysis and manipulation of nanomaterials. It should be noted that Nie *et al*. recently presented a new method to obtain relativistic few-cycle-tunable infrared pulses from a tailored plasma density structure [65]. We believe that the relativistic near-infrared LG laser discussed in this letter can also be implemented as a similar technology to ultimately generate annular attosecond electron slices in experiments in the future.

Acknowledgments

This study was supported by the National Natural Science Foundation of China (grant No. 12075306), Strategic Priority Research Program of the Chinese Academy of Sciences (Grant No. XDB16010600), Key Research Programs in Frontier Science (Grant No. ZDBSLY-SLH006), and Shanghai special science and technology innovation supported project (Grant No. 2019-jmrh1-kj1). Advanced research using high intensity laser produced photons and particles (ADONIS) (CZ.02.1.01/0.0/0.0/16 019/0000789) and High Field Initiative (HiFI) (CZ.02.1.01/0.0/0.0/15 003/0000449), both from European Regional Development Fund. The results of the Project LQ1606 were obtained with the financial support of the Ministry of Education, Youth and Sports as part of targeted support from the National Programme of Sustainability II.

References

1. D. Strickland and G. Mourou, "Compression of Amplified Chirped Optical Pulses," Optics Communications **56**, 3 (1985).
2. Y. X. Leng, "Shanghai Superintense Ultrafast Laser Facility," Chinese Journal of Lasers **46**, 5 (2019).
3. Z. Zhang, F. Wu, J. Hu, X. Yang, J. Gui, P. Ji, X. Liu, C. Wang, Y. Liu, X. Lu, Y. Xu, Y. Leng, R. Li, and

Z. Xu, "The laser beamline in SULF facility," High Power Laser Science and Engineering **8**(2020).

4. F. Lureau, G. Matras, O. Chalus, C. Derycke, T. Morbieu, C. Radier, O. Casagrande, S. Laux, S. Ricaud, G. Rey, A. Pellegrina, C. Richard, L. Boudjemaa, C. Simon-Boisson, A. Baleanu, R. Banici, A. Gradinariu, C. Caldararu, B. D. Boisdeffre, P. Ghenuche, A. Naziru, G. Kolliopoulos, L. Neagu, R. Dabu, I. Dancus, and D. Ursescu, "High-energy hybrid femtosecond laser system demonstrating 2 × 10 PW capability," High Power Laser Science and Engineering **8**(2020).
5. M. Turner and E. Adli and A. Ahuja and O. Apsimon and R. Apsimon and A. M. Bachmann and M. Barros Marin and D. Barrientos and F. Batsch and J. Batkiewicz and J. Bauche and V. K. Berglyd Olsen and M. Bernardini and B. Biskup and A. Boccardi and T. Bogey and T. Bohl and C. Bracco and F. Braunmüller and S. Burger and G. Burt and S. Bustamante and B. Buttenschön and A. Caldwell and M. Cascella and J. Chappell and E. Chevallay and M. Chung and D. Cooke and H. Damerau and L. Deacon and L. H. Deubner and A. Dexter and S. Doebert and J. Farmer and V. N. Fedosseev and G. Fior and R. Fiorito and R. A. Fonseca and F. Friebel and L. Garolfi and S. Gessner and I. Gorgisyan and A. A. Gorn and E. Granados and O. Grulke and E. Gschwendtner and A. Guerrero and J. Hansen and A. Helm and J. R. Henderson and C. Hessler and W. Hofle and M. Hüther and M. Ibison and L. Jensen and S. Jolly and F. Keeble and S. Y. Kim and F. Kraus and T. Lefevre and G. LeGodec and Y. Li and S. Liu and N. Lopes and K. V. Lotov and L. Maricalva Brun and M. Martyanov and S. Mazzoni and D. Medina Godoy and V. A. Minakov and J. Mitchell and J. C. Molendijk and R. Mompo and J. T. Moody and M. Moreira and P. Muggli and E. Öz and E. Ozturk and C. Mutin and C. Pasquino and A. Pardons and F. Peña Asmus and K. Pepitone and A. Perera and A. Petrenko and S. Pitman and G. Plyushchev and A. Pukhov and S. Rey and K. Rieger and H. Ruhl and J. S. Schmidt and I. A. Shalimova and E. Shaposhnikova and P. Sherwood and L. O. Silva and L. Soby and A. P. Sosedkin and R. Speroni and R. I. Spitsyn and P. V. Tuev and F. Velotti and L. Verra and V. A. Verzilov and J. Vieira and H. Vincke and C. P. Welsch and B. Williamson and M. Wing and B. Woolley and G. Xia, "Experimental Observation of Plasma Wakefield Growth Driven by the Seeded Self-Modulation of a Proton Bunch," Physical Review Letters **122**(2019).
6. J. Ren, C. Maurer, P. Katrik, P. M. Lang, A. A. Golubev, V. Mintsev, Y. Zhao, and D. H. H. Hoffmann, "Accelerator-driven high-energy-density physics: Status and chances," Contributions to Plasma Physics **58**, 82-92 (2018).
7. M. Thévenet, A. Leblanc, S. Kahaly, H. Vincenti, A. Vernier, F. Quéré, and J. Faure, "Vacuum laser acceleration of relativistic electrons using plasma mirror injectors," Nature Physics **12**, 355-360 (2015).
8. C. Joshi, W. B. Mori, T. Katsouleas, J. M. Dawson, J. M. Kindel, and D. W. Forslund, "Ultrahigh gradient particle acceleration by intense laser-driven plasma density waves," Nature **311**, 525-529 (1984).
9. S. P. Mangles, C. D. Murphy, Z. Najmudin, A. G. Thomas, J. L. Collier, A. E. Dangor, E. J. Divall, P. S. Foster, J. G. Gallacher, C. J. Hooker, D. A. Jaroszynski, A. J. Langley, W. B. Mori, P. A. Norreys, F. S. Tsung, R. Viskup, B. R. Walton, and K. Krushelnick, "Monoenergetic beams of relativistic electrons from intense laser-plasma interactions," Nature **431**, 535-538 (2004).
10. J. Faure, Y. Glinec, A. Pukhov, S. Kiselev, S. Gordienko, E. Lefebvre, J. P. Rousseau, F. Burgy, and V. Malka, "A laser–plasma accelerator producing monoenergetic electron beams," Nature **431**, 541-544 (2004).
11. C. G. Geddes, C. S. Toth, J. Van Tilborg, E. Esarey, C. B. Schroeder, D. Bruhwiler, C. Nieter, J.

Cary, and W. P. Leemans, "High-quality electron beams from a laser wakefield accelerator using plasma-channel guiding," Nature **431**, 538-541 (2004).

12. E. Esarey, C. B. Schroeder, and W. P. Leemans, "Physics of laser-driven plasma-based electron accelerators," Reviews of Modern Physics **81**, 1229-1285 (2009).
13. X. Wang, R. Zgadzaj, N. Fazel, Z. Li, S. A. Yi, X. Zhang, W. Henderson, Y. Y. Chang, R. Korzekwa, H. E. Tsai, C. H. Pai, H. Quevedo, G. Dyer, E. Gaul, M. Martinez, A. C. Bernstein, T. Borger, M. Spinks, M. Donovan, V. Khudik, G. Shvets, T. Ditmire, and M. C. Downer, "Quasi-monoenergetic laser-plasma acceleration of electrons to 2 GeV," Nat Commun **4**, 1988 (2013).
14. W. P. Leemans, A. J. Gonsalves, H. S. Mao, K. Nakamura, C. Benedetti, C. B. Schroeder, C. Toth, J. Daniels, D. E. Mittelberger, S. S. Bulanov, J. L. Vay, C. G. Geddes, and E. Esarey, "Multi-GeV electron beams from capillary-discharge-guided subpetawatt laser pulses in the self-trapping regime," Phys Rev Lett **113**, 245002 (2014).
15. A. J. Gonsalves, K. Nakamura, J. Daniels, C. Benedetti, C. Pieronek, T. C. H. de Raadt, S. Steinke, J. H. Bin, S. S. Bulanov, J. van Tilborg, C. G. R. Geddes, C. B. Schroeder, C. Tóth, E. Esarey, K. Swanson, L. Fan-Chiang, G. Bagdasarov, N. Bobrova, V. Gasilov, G. Korn, P. Sasorov, and W. P. Leemans, "Petawatt Laser Guiding and Electron Beam Acceleration to 8 GeV in a Laser-Heated Capillary Discharge Waveguide," Phys. Rev. Lett. **122**, 084801 (2019).
16. F. V. Hartemann, S. N. Fochs, G. P. Le Sage, N. C. Luhmann, Jr., J. G. Woodworth, M. D. Perry, Y. J. Chen, and A. K. Kerman, "Nonlinear ponderomotive scattering of relativistic electrons by an intense laser field at focus," Phys Rev E Stat Phys Plasmas Fluids Relat Interdiscip Topics **51**, 4833-4843 (1995).
17. A. Maltsev and T. Ditmire, "Above threshold ionization in tightly focused, strongly relativistic laser fields," Phys Rev Lett **90**, 053002 (2003).
18. X. Cai, J. Zhao, Q. Lin, H. Tong, and J. Liu, "Electron acceleration driven by sub-cycle and single-cycle focused optical pulse with radially polarized electromagnetic field," Opt Express **26**, 30030-30041 (2018).
19. A. Denoeud, L. Chopineau, A. Leblanc, and F. Quere, "Interaction of Ultraintense Laser Vortices with Plasma Mirrors," Phys Rev Lett **118**, 033902 (2017).
20. X.-m. Cai, J.-y. Zhao, Q. Lin, and J.-l. Luo, "Electron acceleration by subcycle pulsed focused vector beams," Journal of the Optical Society of America B **33**(2016).
21. Y. I. Salamin and C. H. Keitel, "Electron acceleration by a tightly focused laser beam," Phys Rev Lett **88**, 095005 (2002).
22. M. C. Downer, R. Zgadzaj, A. Debus, U. Schramm, and M. C. Kaluza, "Diagnostics for plasma-based electron accelerators," Reviews of Modern Physics **90**(2018).
23. J. Schreiber, P. R. Bolton, and K. Parodi, "Invited Review Article: "Hands-on" laser-driven ion acceleration: A primer for laser-driven source development and potential applications," Rev Sci Instrum **87**, 071101 (2016).
24. W. Wang, B. Shen, X. Zhang, L. Zhang, Y. Shi, and Z. Xu, "Hollow screw-like drill in plasma using an intense Laguerre-Gaussian laser," Scientific Reports **5**, 8274 (2015).
25. X. Wang, B. Shen, X. Zhang, W. Wang, J. Xu, L. Yi, and Y. Shi, "High energy protons generation by two sequential laser pulses," Phys. Plasmas **22**, 043106 (2015).
26. W. P. Wang, C. Jiang, H. Dong, X. M. Lu, J. F. Li, R. J. Xu, Y. J. Sun, L. H. Yu, Z. Guo, X. Y. Liang, Y. X. Leng, R. X. Li, and Z. Z. Xu, "Hollow Plasma Acceleration Driven by a Relativistic Reflected Hollow Laser," Physical Review Letters **125**, 034801 (2020).

27. X. Zhang, B. Shen, L. Zhang, J. Xu, X. Wang, W. Wang, L. Yi, and Y. Shi, "Proton acceleration in underdense plasma by ultraintense Laguerre–Gaussian laser pulse," New J. Phys. **16**, 123051 (2014).
28. J. Vieira, J. T. Mendonca, and F. Quere, "Optical Control of the Topology of Laser-Plasma Accelerators," Phys. Rev. Lett. **121**, 054801 (2018).
29. L. X. Hu, T. P. Yu, Z. M. Sheng, J. Vieira, D. B. Zou, Y. Yin, P. McKenna, and F. Q. Shao, "Attosecond electron bunches from a nanofiber driven by Laguerre-Gaussian laser pulses," Scientific Reports **8**, 7282 (2018).
30. C. Baumann and A. Pukhov, "Electron dynamics in twisted light modes of relativistic intensity," Phys. Plasmas **25**, 083114 (2018).
31. L. B. Ju, C. T. Zhou, K. Jiang, T. W. Huang, H. Zhang, T. X. Cai, J. M. Cao, B. Qiao, and S. C. Ruan, "Manipulating the topological structure of ultrarelativistic electron beams using Laguerre–Gaussian laser pulse," New J. Phys. **20**, 063004 (2018).
32. L.-X. Hu, T.-P. Yu, Y. Lu, G.-B. Zhang, D.-B. Zou, H. Zhang, Z.-Y. Ge, Y. Yin, and F.-Q. Shao, "Dynamics of the interaction of relativistic Laguerre–Gaussian laser pulses with a wire target," Plasma Physics and Controlled Fusion **61**, 025009 (2019).
33. J. Vieira and J. T. Mendonça, "Nonlinear Laser Driven Donut Wakefields for Positron and Electron Acceleration," Physical Review Letters **112**, 215001 (2014).
34. H. He, M. E. Friese, N. R. Heckenberg, and H. Rubinsztein-Dunlop, "Direct observation of transfer of angular momentum to absorptive particles from a laser beam with a phase singularity," Phys Rev Lett **75**, 826-829 (1995).
35. L. Allen, M. Beijersbergen, R. Spreeuw, and J. Woerdman, "Orbital angular momentum of light and the transformation of Laguerre-Gaussian laser modes," Phys. Rev. A **45**, 8185-8189 (1992).
36. N. V. Zamfir, "Nuclear Physics with 10 PW laser beams at Extreme Light Infrastructure – Nuclear Physics (ELI-NP)," The European Physical Journal Special Topics **223**, 1221-1227 (2014).
37. Y. Shi, B. Shen, L. Zhang, X. Zhang, W. Wang, and Z. Xu, "Light fan driven by a relativistic laser pulse," Phys Rev Lett **112**, 235001 (2014).
38. W. Gong, B. Shen, L. Zhang, and X. Zhang, "Angular momentum oscillation in spiral-shaped foil plasmas," New Journal of Physics **21**(2019).
39. A. Leblanc, A. Denoeud, L. Chopineau, G. Mennerat, P. Martin, and F. Quéré, "Plasma holograms for ultrahigh-intensity optics," Nature Physics **13**, 440-443 (2017).
40. R. Nuter, P. Korneev, I. Thiele, and V. Tikhonchuk, "Plasma solenoid driven by a laser beam carrying an orbital angular momentum," Physical Review E **98**(2018).
41. J. Vieira, R. M. Trines, E. P. Alves, R. A. Fonseca, J. T. Mendonca, R. Bingham, P. Norreys, and L. O. Silva, "Amplification and generation of ultra-intense twisted laser pulses via stimulated Raman scattering," Nature **7**, 10371 (2016).
42. S. Haddadi, O. Bouzid, M. Fromager, A. Hasnaoui, A. Harfouche, E. Cagniot, A. Forbes, and K. Aït-Ameur, "Structured Laguerre–Gaussian beams for mitigation of spherical aberration in tightly focused regimes," Journal of Optics **20**(2018).
43. A. Pukhov and J. Meyer-ter-Vehn, "Laser wake field acceleration: the highly non-linear broken-wave regime," Applied Physics B: Lasers and Optics **74**, 355-361 (2002).
44. M. Chen, Z.-M. Sheng, Y.-Y. Ma, and J. Zhang, "Electron injection and trapping in a laser wakefield by field ionization to high-charge states of gases," Journal of Applied Physics **99**(2006).

45. T. M. Jeong, S. Bulanov, W. Yan, S. Weber, and G. Korn, "Generation of superposition modes by polarization-phase coupling in a cylindrical vector orbital angular momentum beam," OSA Continuum **2**(2019).
46. W. P. Wang, C. Jiang, B. F. Shen, F. Yuan, Z. M. Gan, H. Zhang, S. H. Zhai, and Z. Z. Xu, "New Optical Manipulation of Relativistic Vortex Cutter," Phys Rev Lett **122**, 024801 (2019).
47. X. Zhang, B. Shen, Y. Shi, X. Wang, L. Zhang, W. Wang, J. Xu, L. Yi, and Z. Xu, "Generation of Intense High-Order Vortex Harmonics," Physical Review Letters **114**, 173901 (2015).
48. L. B. Ju, C. T. Zhou, K. Jiang, T. W. Huang, H. Zhang, T. X. Cai, J. M. Cao, B. Qiao, and S. C. Ruan, "Manipulating the topological structure of ultrarelativistic electron beams using Laguerre–Gaussian laser pulse," New Journal of Physics **20**(2018).
49. S. Li, B. Shen, X. Zhang, Z. Bu, and W. Gong, "Conservation of orbital angular momentum for high harmonic generation of fractional vortex beams," Opt Express **26**, 23460-23470 (2018).
50. L. X. Hu, T. P. Yu, Z. M. Sheng, J. Vieira, D. B. Zou, Y. Yin, P. McKenna, and F. Q. Shao, "Attosecond electron bunches from a nanofiber driven by Laguerre-Gaussian laser pulses," Sci Rep **8**, 7282 (2018).
51. G. Stancari, A. Valishev, G. Annala, G. Kuznetsov, V. Shiltsev, D. A. Still, and L. G. Vorobiev, "Collimation with hollow electron beams," Phys Rev Lett **107**, 084802 (2011).
52. C. J. Zhang, J. F. Hua, Y. Wan, C. H. Pai, B. Guo, J. Zhang, Y. Ma, F. Li, Y. P. Wu, H. H. Chu, Y. Q. Gu, X. L. Xu, W. B. Mori, C. Joshi, J. Wang, and W. Lu, "Femtosecond Probing of Plasma Wakefields and Observation of the Plasma Wake Reversal Using a Relativistic Electron Bunch," Phys Rev Lett **119**, 064801 (2017).
53. T. Z. Zhao, K. Behm, C. F. Dong, X. Davoine, S. Y. Kalmykov, V. Petrov, V. Chvykov, P. Cummings, B. Hou, A. Maksimchuk, J. A. Nees, V. Yanovsky, A. G. Thomas, and K. Krushelnick, "High-Flux Femtosecond X-Ray Emission from Controlled Generation of Annular Electron Beams in a Laser Wakefield Accelerator," Phys Rev Lett **117**, 094801 (2016).
54. A. Forbes, T. E. Lizotte, M. Mousley, G. Thirunavukkarasu, M. Babiker, and J. Yuan, "C-shaped electron beams: design, experimental production and application," in *Laser Beam Shaping XVI,* (2015).
55. T. D. Arber, K. Bennett, C. S. Brady, A. Lawrence-Douglas, M. G. Ramsay, N. J. Sircombe, P. Gillies, R. G. Evans, H. Schmitz, A. R. Bell, and C. P. Ridgers, "Contemporary particle-in-cell approach to laser-plasma modelling," Plasma Physics and Controlled Fusion **57**(2015).
56. A. Henig, S. Steinke, M. Schnurer, T. Sokollik, R. Horlein, D. Kiefer, D. Jung, J. Schreiber, B. M. Hegelich, X. Q. Yan, J. Meyer-ter-Vehn, T. Tajima, P. V. Nickles, W. Sandner, and D. Habs, "Radiation-pressure acceleration of ion beams driven by circularly polarized laser pulses," Phys Rev Lett **103**, 245003 (2009).
57. J. H. Bin, W. J. Ma, H. Y. Wang, M. J. Streeter, C. Kreuzer, D. Kiefer, M. Yeung, S. Cousens, P. S. Foster, B. Dromey, X. Q. Yan, R. Ramis, J. Meyer-ter-Vehn, M. Zepf, and J. Schreiber, "Ion Acceleration Using Relativistic Pulse Shaping in Near-Critical-Density Plasmas," Phys Rev Lett **115**, 064801 (2015).
58. W. P. Wang, B. F. Shen, and Z. Z. Xu, "Accelerating gradient improvement from hole-boring to light-sail stage using shape-tailored laser front," Phys. Plasmas **24**(2017).
59. W. P. Wang, B. F. Shen, X. M. Zhang, L. L. Ji, Y. H. Yu, L. Q. Yi, X. F. Wang, and Z. Z. Xu, "Dynamic study of a compressed electron layer during the hole-boring stage in a sharp-front laser interaction region," Physical Review Special Topics - Accelerators and Beams **15**(2012).

60. W. P. Wang, B. F. Shen, X. M. Zhang, L. L. Ji, M. Wen, J. C. Xu, Y. H. Yu, Y. L. Li, and Z. Z. Xu, "Efficient acceleration of monoenergetic proton beam by sharp front laser pulse," Phys. Plasmas **18**, 013103 (2011).
61. W. Wang, C. Jiang, S. Li, H. Dong, B. Shen, Y. Leng, R. Li, and Z. Xu, "Monoenergetic proton beam accelerated by single reflection mechanism only during hole-boring stage," High Power Laser Sci. Eng. **7**, e55 (2019).
62. Q. Zhan, "Properties of circularly polarized vortex beams," Optics Letters **31**, 3 (2006).
63. W. P. Wang, B. F. Shen, X. M. Zhang, L. L. Ji, Y. H. Yu, L. Q. Yi, X. F. Wang, and Z. Z. Xu, "Dynamic study of a compressed electron layer during the hole-boring stage in a sharp-front laser interaction region," Phys. Rev. ST Accel. Beams **15**, 081302 (2012).
64. W. P. Wang, B. F. Shen, and Z. Z. Xu, "Accelerating gradient improvement from hole-boring to light-sail stage using shape-tailored laser front," Phys. Plasmas **24**, 013104 (2017).
65. Z. Nie, C.-H. Pai, J. Hua, C. Zhang, Y. Wu, Y. Wan, F. Li, J. Zhang, Z. Cheng, Q. Su, S. Liu, Y. Ma, X. Ning, Y. He, W. Lu, H.-H. Chu, J. Wang, W. B. Mori, and C. Joshi, "Relativistic single-cycle tunable infrared pulses generated from a tailored plasma density structure," Nature Photonics **12**, 489-494 (2018).